Land-based wind plant wake characterization using dual-Doppler radar measurements at AWAKEN

Journal of Physics: Conference Series **2767** (2024) 092037 doi:10.1088/1742-6596/2767/9/092037

Land-based wind plant wake characterization using dual-Doppler radar measurements at AWAKEN

Aliza Abraham[1], Nicholas Hamilton[1], Nicola Bodini[1], Brian Hirth[2], John Schroeder[2], Stefano Letizia[1], Raghavendra Krishnamurthy[3], Rob Newsom[3], Patrick Moriarty[1]

[1] National Renewable Energy Laboratory, Golden, CO, USA
[2] Texas Tech University, Lubbock, TX, USA
[3] Pacific Northwest National Laboratory, Richland, WA, USA

E-mail: aliza.abraham@nrel.gov

Abstract. Wind plant wakes have been shown to persist for tens of kilometers downstream in offshore environments, reducing the power output of neighboring plants, but their behavior on land remains relatively unexplored through observation. This study capitalizes on the unique and extensive field data collected for the American WAKE ExperimeNt (AWAKEN) project underway in northern Oklahoma. X-band dual-Doppler radars deployed at this site measure wind speed and direction at 25-m and 2-min resolution within a 30-km range, capturing the interactions between three neighboring wind plants. These measurements show that the wake of one wind plant extends at least 15 km downstream under easterly wind and stable atmospheric conditions. Though the wake wind speed increases within the first 10 km, it plateaus at 90% of the freestream wind speed. The spanwise velocity distribution within the wake initially shows the clear signature of the wind plant layout, which is smoothed as it propagates downstream, indicating spanwise momentum transfer is a key mechanism in wind plant wake development and recovery. These findings have important implications for wind plant siting decisions and resource assessments, and provide insights into atmospheric interactions at the wind plant scale.

1. Introduction

As wind energy deployment continues to increase, so does the need to understand the behavior of wind plant wakes, the regions of lower wind speed and higher turbulence behind clusters of wind turbines. Areas with strong wind resources, such as the Great Plains region of the United States, are highly sought-after for wind plant deployments, leading to the construction of multiple wind plants within close proximity of each other. In these situations, the wakes of adjacent plants can cause reduced power output [1] and increased fatigue loading for their neighbors [2]. Furthermore, wind plant wakes have been observed to persist for tens of kilometers downstream, especially for offshore plants [2]. Studies have also shown that wind plant wakes impact the surrounding atmospheric [3] and surface conditions, with agricultural and environmental implications [4]. For these reasons, improved characterization of wind plant wakes was identified as the highest-priority testable hypothesis for the multi-institutional American WAKE experimeNt field campaign (AWAKEN [5]).

While individual turbine wakes have been studied extensively, plant wakes have received less attention. Because the physical scales of the problem span such a large range, it is difficult to

study wind plant wakes using laboratory-scale experiments and numerical simulations. Some field-scale studies have been conducted, primarily in offshore environments. Christiansen and Hasager [6] observed velocity deficits behind offshore wind plants using synthetic aperture radar (SAR) measurements from satellites, and Nygaard [7] quantified efficiency losses and turbulence increases between neighboring wind plants using turbine supervisory control and data acquisition (SCADA) data. In attempts to evaluate the maximum extent of wind plant wakes, Platis et al. [2] and Nygaard and Newcombe [8] used aircraft measurements and dual-Doppler radar with domains reaching 45 km and 17 km, respectively, downstream of offshore wind plants, but found that the wakes extended beyond their measurement domains. Schneemann et al. [9] observed the wake of an offshore wind plant extending at least 55 km downstream, with a velocity deficit consistently greater than 20%, using long-range lidar and satellite SAR measurements. In a land-based study, Lundquist et al. [1] employed a combination of wind plant operational data and econometric and atmospheric models to estimate 5% losses in power generation at a downwind plant due to wake effects from its upstream neighbor. Bodini et al. [3] compared pre- and post-construction velocity profiles 3.5 km downstream of a land-based wind plant, observing a velocity deficit up to 6% and an increase in turbulent kinetic energy (TKE) of more than 30% under stable atmospheric conditions.

Models have been developed to represent these observed wind plant wake effects at different levels of fidelity. Nygaard et al. [10] adapted the analytical Park model to turbine clusters by incorporating atmospheric and wake-added turbulence. Preliminary comparisons between this TurbOPark model and offshore wind plant SCADA data revealed the need for further validation and calibration. Fitch et al. [11] developed a widely-used wind farm parameterization for the Weather Research and Forecasting (WRF) model which represents turbines as momentum sinks and TKE sources. Results from WRF using this parameterization showed wind plant wakes extending up to 90 km downstream and reducing power production of neighboring turbines by one third off the U.S. east coast [12]. However, in a WRF validation study against lidar and aircraft data captured in the German Bight, Cañadillas et al. [13] found wind speed disagreements of nearly 20% between the model and measurements. While higher-fidelity models such as the Reynolds-Averaged Navier-Stokes (RANS) method have the ability to represent more of the wind turbine physics, they are computationally expensive to run. To lower this cost, van der Laan et al. [14] proposed a strategy for modeling wind plants as a forest canopy. The proposed method compared well with the RANS model with individual turbines represented as actuator disks, but significant disagreements were found between the RANS, WRF, and TurbOPark models. These disagreements demonstrate the importance of collecting additional field data for model validation and improvement, and for increased understanding of the physics governing wind plant wake behavior.

As part of the AWAKEN campaign, a field site encompassing five neighboring wind plants is heavily instrumented with *in situ* and remote-sensing devices [15]. One such remote-sensing system is the X-band dual-Doppler radar [16], which uses coordinated measurements of two Doppler radars to reconstruct both horizontal velocity components within a volume. By generating signals with frequencies in the X-band, the sensor range extends more than 30 km. At AWAKEN, the X-band radar field of view covers three wind plants and their surroundings, spanning 225 m of height. The current study employs observations from the radars, alongside the other instruments at the field site, to measure the magnitude and extent of the wind plant wake. We further aim to understand how factors such as wind plant layout and atmospheric conditions affect wake development and evolution. This manuscript is organized as follows: Section 2 describes the experimental methods used in the study; Section 3 presents the results of the investigation, highlighting the velocity distribution in the wind plant wake, and discusses their implications; and Section 4 provides a summary of key findings, along with some concluding remarks.

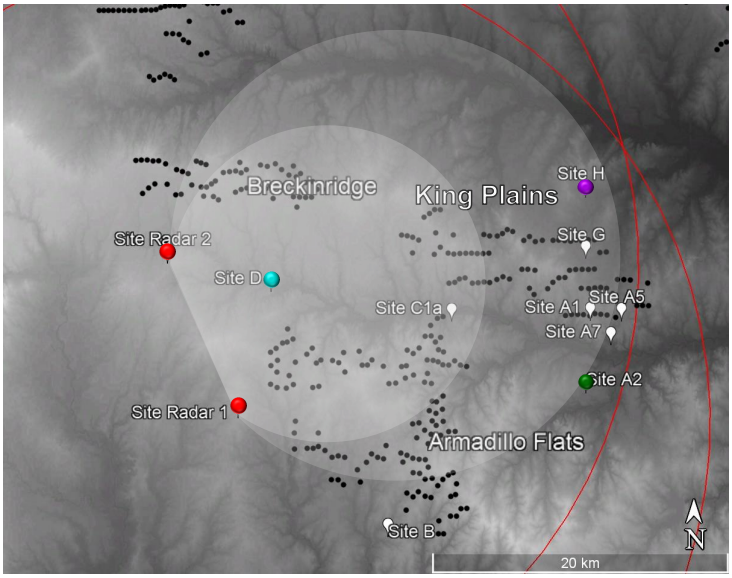

Figure 1. Map of the AWAKEN site highlighting the dual-Doppler radar field of view. The two radars are shown as red dots and their radial range is indicated by red lines. Wind turbines are shown as black dots and wind plants are labeled by name. Ground-based measurement sites are labeled by letter and indicated with white pins. The sites of ground-based lidars used for further analysis in the current study are marked by colored dots (cyan, purple, and green). The lightly shaded circle indicates the extent of the radar coarse-resolution grid while the more intensely shaded circle marks the extent of the fine-resolution grid. The shading in the background represents the terrain.

2. Experimental methods

2.1. AWAKEN field site

The AWAKEN field campaign has been underway in northern Oklahoma since the fall of 2022, spanning a region of more than 1000 km^2 near the Atmospheric Radiation Measurement Southern Great Plains site. The land use in the region is primarily agricultural and terrain is relatively smooth, with less than 80 m height difference between the lowest and highest points at the site. The wind turbine locations at the site are shown as black dots in Figure 1. The primary focus of the current investigation is the wake of the King Plains wind plant, the newest wind plant in the area. This plant is composed of 88 GE 2.82-MW turbines, with hub heights of 89 m and rotor diameters of 127 m [17]. The locations of ground-based instruments used in the AWAKEN campaign are also shown on the map in Figure 1.

2.2. X-band dual-Doppler radar measurements

The two X-band radars in the dual-Doppler system used in the AWAKEN campaign are configured to scan overlapping horizontal sectors of 145° at 30°/s, with 0.35° steps, at 18 elevation angles between 0° and 2°. This scan pattern takes each radar 124 seconds to complete. Because the two radars are not synchronized, the resulting temporal resolution of the dual-Doppler velocity field is between 2 and 4 min. The beam width is 0.5° in the azimuthal and elevation dimensions. The azimuthal pointing angle was aligned using 20 nearby turbines as hard targets, yielding an accuracy within 0.05°. The elevation angle was calibrated with a high-precision digital level to an accuracy within 0.02°. In the radial direction, the maximum measurement range of each X-band radar is extended by an order of magnitude relative to the previous Ka-band version, up to 30 km. The range gate length and spacing are both 9 m in the

radial direction.

A real-time quality control procedure is applied to remove data with low signal power as well as adverse velocity influences of non-meteorological targets and ground clutter, then the radial velocities are interpolated to two Cartesian grids, one fine and one coarse. The fine grid, with a horizontal resolution of 25 m, covers the region closest to the radars where the signal is strongest (intensely shaded circle in Figure 1). The coarse grid covers the whole domain with a 50 m horizontal resolution (lightly shaded circle in Figure 1). Both grids have a resolution of 25 m in the vertical direction, ranging from 375 m to 600 m (with an average terrain height of 329 m) above mean sea level (MSL). Dual-Doppler synthesis is then performed to reconstruct horizontal velocity vectors from the radial velocities measured by both radars. The uncertainty in the velocity introduced by dual-Doppler synthesis depends on the wind direction and beam crossing angle [18]. In the fine grid region under the easterly wind conditions selected for the current investigation, this geometric uncertainty is much lower than the statistical variability represented by the error bars throughout the manuscript. For the current study, the dual-Doppler velocity profiles are interpolated from MSL-relative heights to heights above ground level (AGL, from 45 m to 270 m, preserving the 25-m resolution) in order to account for variations in terrain. Though terrain changes are moderate, even small height differences can cause over- or under-estimation of wind speeds if neglected, especially under strong shear conditions [19].

2.3. Radar data selection

Conditional sampling of the radar data collected between June 1 and October 8, 2023, was performed based on wind direction, atmospheric stability, and turbine operation. For the AWAKEN campaign, the radars were configured to capture the interactions between the three wind plants, King Plains, Armadillo Flats, and Breckinridge, within the fine grid measurement region (Figure 1). In order to capture the maximum length of the wake within the fine grid region, the current study focuses on characterizing the wake of King Plains under easterly wind conditions ($90^\circ \pm 10^\circ$ clockwise from north), when the wake extends west toward the radars. The hub-height inflow wind direction used for sampling was measured by scanning lidars operated in profiling mode at sites A1, A2, and H. In addition, to capture the wake at maximum strength and persistence, stable atmospheric conditions were selected [20], as determined by the Obukhov length, L, in the range 0 m $< L <$ 600 m [21]. Measurements from surface flux stations at sites A1, A2, A5, and G were used to compute L at 30-min resolution. The data selected was restricted to periods when at least 80% of the turbines in King Plains were operating normally, i.e., between cut-in and cut-out, and without curtailment. Periods of curtailment were identified based on the deviation of the generated power and wind speed recorded by the turbine SCADA from the expected power curve. Note that turbine thrust coefficient was not included in the data selection procedure, as limiting the allowable wind speed range too much would substantially reduce data availability. However, the radar velocity fields recorded during each selected period were manually inspected to confirm the presence of a clear velocity deficit in the wake of King Plains. Finally, to prevent transient phenomena within the domain from dominating the ensemble average, a minimum duration restriction of 30 min where the above conditions were met and dual-Doppler radar data was available was instated. Nine periods of $\geq$30 min were identified that met these criteria, for a total of 852 min.

2.4. Ground-based lidar measurements

Ground-based lidars at sites A2, D, and H (green, cyan, and purple dots in Figure 1, respectively) were used to validate and supplement the radar measurements. The Halo XR and XR+ scanning lidars at A2 and H, respectively, perform a six-beam profiling scan to record inflow wind speed and direction under the easterly wind conditions investigated here. These profiles are stored at 10-min temporal and 10-m spatial resolution, spanning 90 m to 4000 m AGL. Dynamic

filtering is applied to the scanning lidar data, following the approach described by Beck and Kühn [22]. A Windcube profiling lidar is located at site D, in the wake of King Plains, recording wind speed and direction at ∼1-s temporal resolution. The spatial resolution is 10 m from 40 m to 100 m AGL, then 20 m for heights between 100 m and 200 m AGL. These data are filtered by removing periods when the carrier-to-noise ratio drops below -20 dB. For the current investigation, ensemble averages of the lidar velocities are calculated over the periods identified in Section 2.3, with the additional criteria of lidar data availability, for direct comparison with the radar data.

3. Results and discussion

The wind plant wake is clearly visible in the dual-Doppler horizontal velocity field obtained by the radars. In the example frame shown in Figure 2a, taken at the elevation nearest turbine hub height (80 m AGL), easterly wind causes the low-velocity region to extend west of King Plains to the western edge of the measurement domain, a distance of at least 15 km. The effects of plant layout are also visible, with bands of low-speed flow emanating from turbine rows, and higher-speed flow persisting between rows. The ensemble-averaged velocity field of the periods identified in Section 2.3 (i.e., wind from the east and stable atmospheric boundary layer) is presented in Figure 2b. Before averaging, the mean hub-height inflow wind speed, U_∞, is calculated for each period from the radar data, then used to normalize the velocity fields for that period. The computation of the inflow wind speed profile from the radar velocity fields is discussed in Section 3.1. The same features observed in the instantaneous snapshot can be detected in the mean, though they are smoothed out by turbulence and mesoscale flow variability. The following analysis will focus on certain aspects of the mean flow field, marked by symbols in Figure 3, where x is the streamwise distance from the westernmost turbine in the King Plains wind plant, and y is the spanwise distance from the center of the plant in the north-south direction.

3.1. Comparison with lidar

First we present a comparison between wind speed and direction profiles measured by the radar system and the ground-based lidars at the site. Because the radars do not measure the flow upstream of King Plains within the fine grid region when the wind is from the east, a region north of the wind plant, marked by a blue box in Figure 3, is used as the reference (inflow) velocity for the radar data. Figure 4a compares the mean wind speed and direction within this box with the inflow measurements recorded by the scanning lidars at sites A2 and H (green and purple dots in Figure 1, and outside the domain of Figure 3). Although these sites are not co-located with the radar inflow region, all three are undisturbed by wind turbine wakes under easterly wind conditions, and are therefore expected to show reasonable agreement. Averages are calculated over seven of the nine periods identified in Section 2.3; two are excluded where high-quality data are not available from one of the lidars. Note that the radar profiles have larger error bars than those for the lidar because they include the spatial variability within the 5 km × 5 km horizontal region demarcated by the blue box, whereas the lidars measure over a much smaller horizontal region determined by their conical scanning pattern. At the heights where the radar and lidar measurements overlap, the wind direction compares well. The wind speed is slightly overestimated by the radar relative to the lidars, with larger differences observed at lower elevations. The overestimation is attributed to the radar data grid interpolation process. Because the radar beams are 0.5° wide, the area each beam covers increases with distance from the radar. Where the beam area is large (farther away from the radars) and when background return power is relatively low, ground clutter affects velocity measurements at lower tilt angles, which are then removed by the quality control procedure. As a result, velocity values at a given grid point are biased toward a higher altitude, and therefore a higher magnitude under

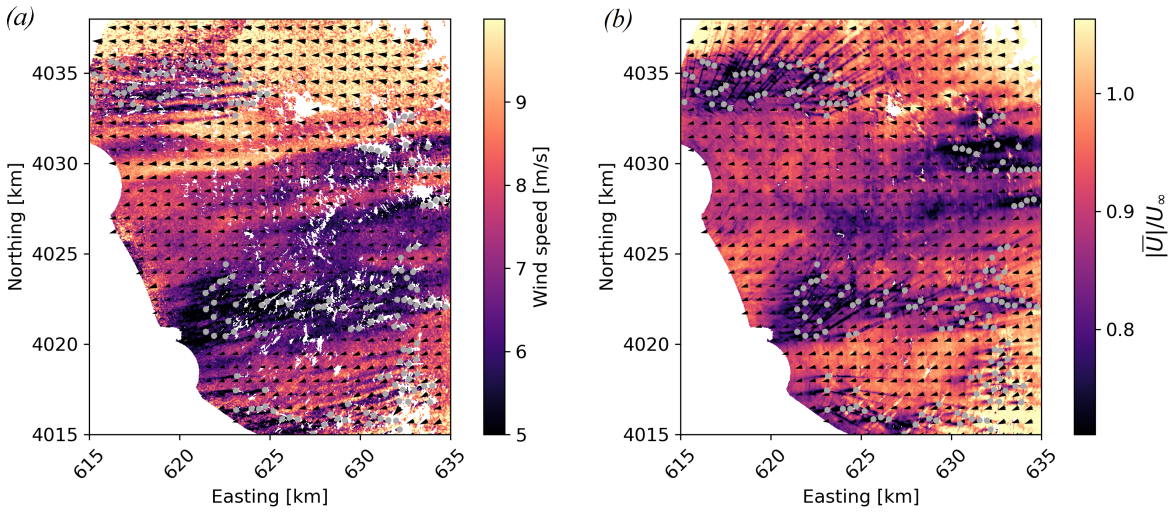

Figure 2. (a) Instantaneous (captured between 05:12 and 05:16 UTC on June 15, 2023) and (b) ensemble-averaged velocity field at 80 m AGL for the conditions described in Section 2.3 (wind from the east, stable atmospheric boundary layer), captured within the fine grid measurement region of the dual-Doppler radars at the AWAKEN site. The velocity magnitude is $|U|$, and the overbar denotes an ensemble average. Streaks extending along the radial line from the radars to the turbines are artifacts caused by range-time sidelobes from pulse compression. Gray dots mark turbine locations. Black vectors showing wind velocity magnitude and direction are shown every 30 grid points to facilitate visibility. Northing and easting are in UTM coordinates.

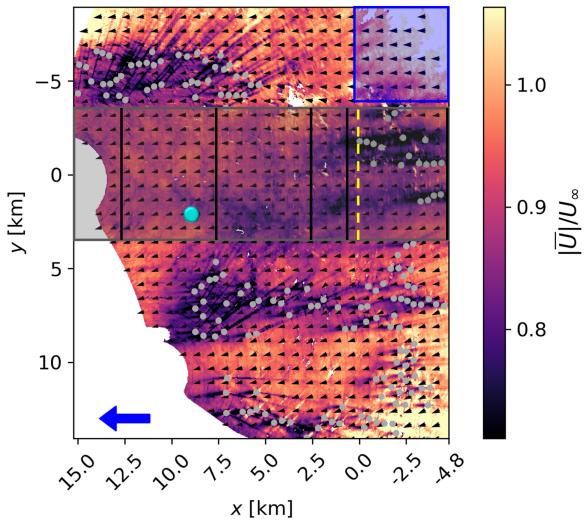

Figure 3. Ensemble-averaged radar velocity field with the coordinate system defined relative to the westernmost turbine in the King Plains wind plant (dashed yellow line) in the streamwise direction (x) and the center of the plant in the spanwise direction (y). The blue arrow indicates the wind direction and the other annotations indicate measurement locations discussed throughout the manuscript.

conditions of wind speed shear, as in the lower part of the profile in Figure 4a.

Figure 4b compares radar and lidar measurements in the wake, taken from the profiling lidar at site D (marked by the cyan dot in Figure 3) and the nearest fine grid radar data point. In this case, averages are calculated using eight of the nine periods from Section 2.3, with one removed due to lack of lidar data availability. Here, the wind speed profiles exhibit better agreement than in the inflow for two reasons. First, the wake radar and lidar measurements are co-located, whereas the inflow measurements are not. Second, the measurement location is closer to the

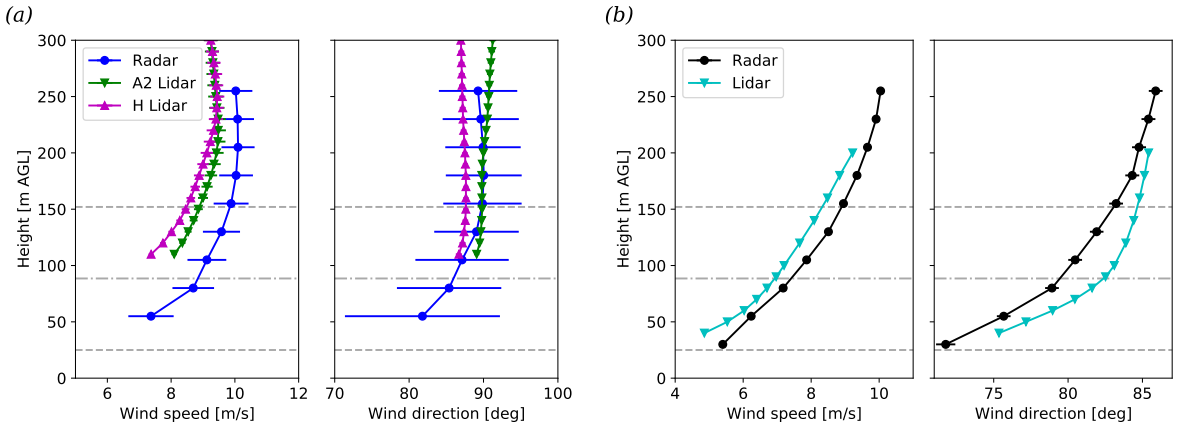

Figure 4. Comparison of ensemble-averaged wind speed and direction profiles from radar and lidar (a) in the inflow and (b) in the wind plant wake. Error bars represent the standard error of the measurements. Dot-dashed lines indicate the King Plains turbine hub height, and dashed gray lines indicate the top and bottom rotor tips.

radars, so the beam area is smaller and the upward bias introduced by the grid interpolation process is weaker. Still, a slight difference in wind speed and direction is observed between the radar and lidar measurements. Further investigation is underway to better understand these deviations.

3.2. Streamwise wake evolution

Figure 5 shows the evolution of the wind speed around hub height (80 m AGL) with downstream distance from the plant. The black line is computed as the mean of the data within the gray box in Figure 3, taken in the north-south direction such that variations in the east-west direction are visible. The spanwise extent of this region is bounded by the north- and south-most turbines in the King Plains wind plant. The streamwise extent is limited by the size of the fine grid radar domain and includes the westernmost 4.8 km of the wind plant and 15.2 km downstream. The blue line is the mean of the wind speed within the reference region of the radar at 80 m AGL. This plot shows that the velocity deficit increases slightly in the streamwise direction within the last few kilometers of the plant until it reaches a magnitude of $\sim 0.2U_\infty$. After the flow leaves the last row of the plant, the velocity increases for 10 km downstream, at which point it stays relatively constant at $\sim 0.9U_\infty$ until the edge of the radar domain. The flow does not fully recover to the inflow wind speed within this 15-km distance.

3.3. Vertical distribution of wake velocity

Previous studies have indicated that, within large wind plants, the entrainment of kinetic energy from above the plant is primarily responsible for energizing the flow and allowing turbines deep within the array to generate power [23, 24]. Therefore, we look to the vertical distribution of velocity within the wind plant wake to investigate its effect on wake recovery. Figure 6a shows a series of spanwise-vertical planes at different streamwise distances from the downstream edge of the wind plant (plane locations are indicated by black lines in Figure 3), alongside the wind speed profiles computed as the spanwise mean of each plane. These profiles are plotted with the radar reference wind speed profile for comparison. The velocity deficit induced by the wind plant wake exists mostly within the heights of the turbine rotors, but it persists with decreasing magnitude until ~100 m above the rotor top tips, suggesting momentum has been transferred from the flow above the plant to replenish the energy extracted by the turbines. As downstream

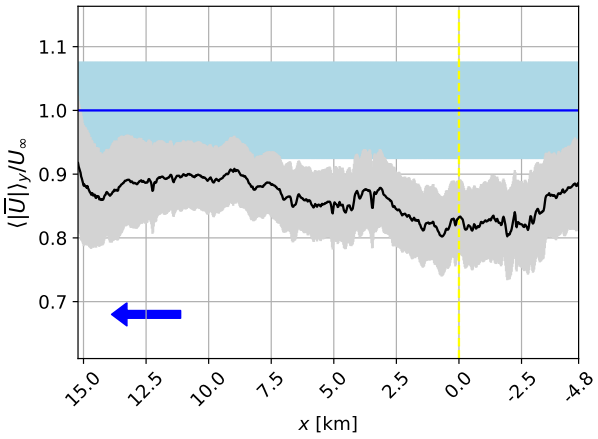

Figure 5. Mean wind plant wake velocity (black) compared with mean reference velocity (blue) from the radars at 80 m AGL. The $\langle\rangle_y$ denotes a spatial average in the y direction. The shaded regions represent the standard error of the measurements. The blue arrow indicates the direction of the flow and the yellow dashed line marks the downstream (western) boundary of the wind plant.

distance increases, the wake velocity profiles begin to approach the inflow wind speed, exhibiting partial wake recovery. However, at $x = 12.7$ km, the farthest downstream distance where radar data is available above hub height, a velocity deficit is still observed between hub height and top tip height. At the lowest altitudes, the profiles exhibit a slight increase in velocity deficit with downstream distance, though this effect is likely due to variations in surface roughness caused by small changes in terrain or land use within the domain.

3.4. Spanwise wake variation

Spanwise velocity variations are also visible in the planes shown in Figure 6a. Figure 6b highlights the distribution of these variations by presenting a cross section of each plane at turbine hub height. The plane most upstream is taken within the wind plant, 4.8 km upstream of the last turbine and at the eastern boundary of the radar's fine grid region. As shown in Figure 3, this plane cuts through two turbine rows, whose signatures are clearly visible in the wind speed profile as two deep wind speed troughs. In the first plane downstream of the wind plant (0.6 km), the strength of these troughs is significantly reduced, but the spanwise variation of the velocity caused by the layout of the wind plant rows is still visible. As downstream distance increases, the spanwise variations decrease, until the velocity is nearly uniform in the spanwise direction at 7.6 km downstream of the plant. This evolution of the spanwise velocity profiles indicates spanwise momentum transfer is occurring between low- and high-speed regions in the wake, smoothing out the velocity distribution. The contribution of spanwise momentum transfer to the wind plant wake velocity distribution measured in the current study suggests that it could be an important mechanism for wake recovery. Furthermore, when the wind is from the east at the AWAKEN site, the wake of King Plains is bounded by two other wind plants to the north and south, which also generate low-momentum regions. These wind plants prevent the entrainment of higher momentum flow into the King Plains wake from the spanwise directions, likely inhibiting full wake recovery, as observed from the plateau in the mean streamwise velocity presented in Section 3.2.

4. Conclusion

The current study uses dual-Doppler X-band radar measurements from the AWAKEN field campaign to characterize wind plant wakes. The radar system measures the wind speed and direction over a >30 km range, capturing the region between three wind plants in northern Oklahoma. These data are sampled for stable atmospheric conditions ($0 \text{ m} < L < 600 \text{ m}$) and easterly wind directions ($90° \pm 10°$), where the wake of one plant is visible within the

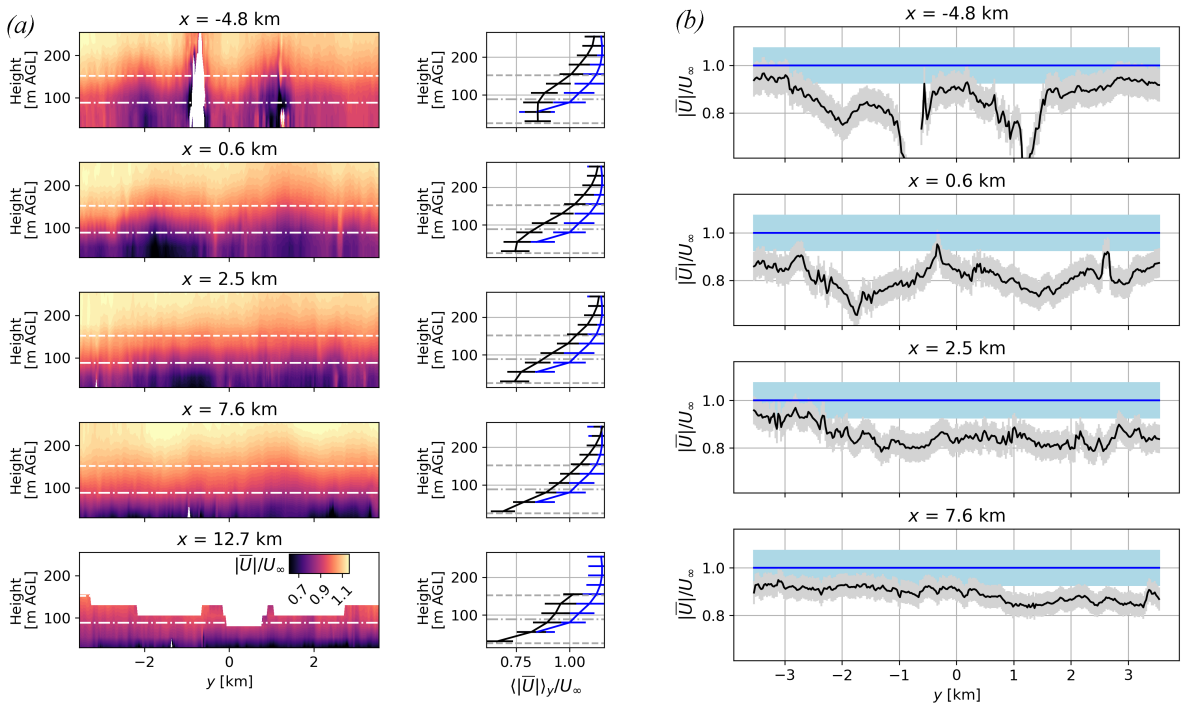

Figure 6. (a) The left column shows spanwise-vertical planes of mean horizontal velocity magnitude at different downstream locations in the wind plant wake, indicated by black lines in Figure 3. The dot-dashed and dashed white lines indicate hub and top-tip heights, respectively, of the King Plains turbines. The right column shows the spanwise mean of each plane in black, with the mean reference wind speed profile from the radars in blue. Dot-dashed and dashed gray lines indicate turbine hub and top- and bottom-tip heights, respectively. (b) Black lines are spanwise cross sections of the first four planes in panel (a), taken at the radar measurement height nearest hub height (80 m AGL). Blue lines represent the reference wind speed. The shaded regions indicate the standard error of the measurements.

radar domain, and the 852 min of data meeting these criteria are normalized by inflow wind speed and averaged. Under these conditions, the wind speed and direction profiles measured by the radar are shown to agree reasonably well with ground-based lidar measurements, with some deviations that are under further investigation. Using the ensemble-averaged radar data, the plant wake velocity distributions in the streamwise, vertical, and spanwise directions are investigated. Results show that the wake velocity recovers up to 90% of the inflow wind speed within the first 10 km downstream of the plant, then plateaus. Strong variations are observed in the spanwise velocity distribution, showing the clear signature of the wind plant layout. These variations are smoothed out with downstream distance, highlighting the importance of spanwise momentum transfer within the wake. Furthermore, the wind plants on either side of the wake under easterly wind conditions, blocking spanwise momentum transfer into the wake, are proposed as an explanation for the lack of full wake recovery observed.

These findings have important implications for wind plant siting decisions and energy production estimates. According to the U.S. Wind Turbine Database hosted by the U.S. Geological Survey [17], many land-based wind plants are already located within 15 km of each other, particularly in the Midwest and Great Plains regions of the United States. The results of the current study show that the wind plant wake can reduce wind speeds, and thereby energy available to neighboring wind plants, for at least 15 km downstream. In addition, if the wake

passes between other wind plants, wake recovery could be inhibited. These effects must be considered when selecting the locations for new wind plants and when conducting wind resource assessments in regions densely populated with wind turbines.

The results of this study will also be used for benchmarking efforts to validate numerical models across a range of fidelities as part of the AWAKEN project. The findings of this study highlight the importance of including features such as terrain and nearby wind plants in the models. Combining experimental data with model results provides the opportunity to better understand the wake behaviors observed in the current study and to validate the explanations proposed for these observations. Further analysis of the data recorded by other instruments at the site will also provide additional insight into the phenomena discussed here. In particular, ground-based and nacelle-mounted lidars will be used in tandem to quantify momentum transfer at locations upstream, between rows, and within the wake of the wind plant. This work advances our understanding of atmospheric interactions at the wind plant scale, listed as one of the grand challenges of wind energy [25], pushing wind energy closer to reaching its full potential.

4.1. Acknowledgments

This work was authored in part by the National Renewable Energy Laboratory, operated by Alliance for Sustainable Energy, LLC, for the U.S. Department of Energy (DOE) under contract no. DE-AC36-08GO28308. Funding was provided by the U.S. Department of Energy Office of Energy Efficiency and Renewable Energy Wind Energy Technologies Office. The views expressed in the article do not necessarily represent the views of the DOE or the U.S. Government. The U.S. Government retains and the publisher, by accepting the article for publication, acknowledges that the U.S. Government retains a nonexclusive, paid-up, irrevocable, worldwide license to publish or reproduce the published form of this work, or allow others to do so, for U.S. Government purposes. PNNL is operated for DOE by the Battelle Memorial Institute under Contract DE-AC05-76RLO1830. The provision of the profiling lidar at site D was financed by the German Federal Ministry for Economic Affairs and Climate Action (BMWK) as part of the project Windpark Radar (funding code 03EE3031A).

References

[1] Lundquist J K, DuVivier K K, Kaffine D and Tomaszewski J M 2019 *Nat. Energy* **4** 26–34
[2] Platis A *et al.* 2018 *Sci. Rep.* **8** 2163
[3] Bodini N, Lundquist J K and Moriarty P 2021 *Sci. Rep.* **11** 22939
[4] Rajewski D A *et al.* 2013 *Bull. Am. Meteorol. Soc.* **94** 655–72
[5] Moriarty P, Hamilton N, Debnath M, Herges T, Isom B, Lundquist J K, Maniaci D, Naughton B, Pauly R, Roadman J and Shaw W 2020 American wake experiment (awaken) (nrel/tp-5000-75789) Tech. Rep. NREL/TP-5000-75789 National Renewable Energy Lab.(NREL) Golden, CO (United States)
[6] Christiansen M B and Hasager C B 2005 *Remote Sens. Environ.* **98** 251–68
[7] Nygaard N G 2014 *J. Phys.: Conf. Ser.* **524** 012162
[8] Nygaard N G and Newcombe A C 2018 *J. Phys.: Conf. Ser.* **1037** 072008
[9] Schneemann J, Rott A, Dörenkämper M, Steinfeld G and Kühn M 2020 *Wind Energy Sci.* **5** 29–49
[10] Nygaard N G, Steen S T, Poulsen L and Pedersen J G 2020 *J. Phys.: Conf. Ser.* **1618** 062072
[11] Fitch A C, Olson J B, Lundquist J K, Dudhia J, Gupta A K, Michalakes J and Barstad I 2012 *Mon. Weather Rev.* **140** 3017–38
[12] Pryor S C, Barthelmie R J and Shepherd T J 2021 *Joule* **5** 2663–86
[13] Cañadillas B, Beckenbauer M, Trujillo J J, Dörenkämper M, Foreman R, Neumann T and Lampert A 2022 *Wind Energy Sci.* **7** 1241–62
[14] van der Laan M P, García-Santiago O, Kelly M, Meyer Forsting A, Dubreuil-Boisclair C, Sponheim Seim K, Imberger M, Peña A, Sørensen N N and Réthoré P E 2023 *Wind Energy Sci.* **8** 819–48
[15] Debnath M *et al.* 2022 *J. Phys.: Conf. Ser.* **2265** 022058
[16] Hirth B D, Schroeder J L and Guynes J G 2017 *J. Phys.: Conf. Ser.* **926** 012003
[17] Hoen B D, Diffendorfer J E, Rand J T, Kramer L A, Garrity C P and Hunt H E 2018 United states wind turbine database v6.1 (november 28, 2023): U.s. geological survey, american clean power association, and lawrence berkeley national laboratory data release URL `https://eerscmap.usgs.gov/uswtdb/`

[18] Stawiarski C, Träumner K, Knigge C and Calhoun R 2013 *J. Atmos. Ocean. Tech.* **30** 2044–62
[19] Sanchez Gomez M, Lunquist J K, Mirocha J D, Arthur R S, Muñoz-Esparza D and Robey R 2022 *J. Renew. Sustain. Energy* **14** 063303
[20] Magnusson M and Smedman A S 1994 *Wind Eng.* **18**(3) 139–52
[21] Wharton S and Lundquist J K 2012 *Wind Energy* **15**(4) 525–46
[22] Beck H and Kühn M 2017 *Remote Sens.* **9** 561
[23] Calaf M, Meneveau C and Meyers J 2010 *Phys. Fluids* **22** 015110
[24] Cal R B, Lebrón J, Castillo L, Kang H S and Meneveau C 2010 *J. Renew. Sustain. Energy* **2** 013106
[25] Veers P *et al.* 2019 *Science* **366** eaau2027